STAR-RIS-NOMA Networks: An Error Performance Perspective

Mahmoud Aldababsa, Aymen Khaleel, *Graduate Student Member, IEEE*
and Ertugrul Basar, *Senior Member, IEEE*

***Abstract*—This letter investigates the bit error rate (BER) performance of simultaneous transmitting and reflecting reconfigurable intelligent surfaces (STAR-RISs) in non-orthogonal multiple access (NOMA) networks. In the investigated network, a STAR-RIS serves multiple non-orthogonal users located on either side of the surface by utilizing the mode switching protocol. We derive the closed-form BER expressions in perfect and imperfect successive interference cancellation cases. Furthermore, asymptotic analyses are also conducted to provide further insights into the BER behavior in the high signal-to-noise ratio region. Finally, the accuracy of our theoretical analysis is validated through Monte Carlo simulations. The obtained results reveal that the BER performance of STAR-RIS-NOMA outperforms that of the classical NOMA system, and STAR-RIS might be a promising NOMA 2.0 solution.**

***Index Terms*—Bit error rate, non-orthogonal multiple access, simultaneous transmitting and reflecting reconfigurable intelligent surface, successive interference cancellation.**

I. Introduction

NON-ORTHOGONAL multiple access (NOMA) has been recognized as a promising multiple access candidate to satisfy the challenging requirements of sixth-generation wireless networks such as high spectral efficiency, massive connectivity, and low latency [1]. Different from conventional orthogonal multiple access (OMA), in which different users are allocated to different resource blocks (time, frequency, code), NOMA can accommodate multiple users via the same resource block, which effectively enhances the spectral efficiency. In power-domain (PD)-NOMA, users are assigned to different power levels, and the signals of all users are superimposed into a single message transmitted from the base station (BS). At the receiver side, successive interference cancellation (SIC) is applied to eliminate the inter-user interference and to recover the transmitted symbol [2]. In [3], the authors analyzed the bit error rate (BER) performance of uplink and downlink NOMA networks, where a binary phase shift keying (BPSK) and quadrature phase shift keying modulation schemes are employed for the far and near users, respectively. In [4], the closed-form expressions are derived for the BER of a two-user non-orthogonal NOMA system using quadrature amplitude modulation. In [5], the authors proposed a multi carrier-based technique that combines both transmit diversity and NOMA protocol, resulting in enhancing both reliability and sum-rate performance.

Reconfigurable intelligent surfaces (RISs) have also attracted attention as a promising candidate for next generation wireless communication networks. An RIS consists of a massive number of low-cost passive elements that reconfigure the propagation of incident wireless signals by adjusting each element's amplitude and phase shift. In [6], the authors maximized the sum throughput for an RIS-assisted internet-of-things network by jointly optimizing the RIS passive beamforming vector, the transfer time scheduling, and power splitting ratio, under energy harvest-then-transmit policy protocol. In [7]-[8], the authors analyzed the BER for a RIS-assisted NOMA system, where the RIS is partitioned into multiple subsurfaces, each allocated to serve a single user. It is worthing to mention that RISs can only serve the users located on the same side of the surface. Nevertheless, simultaneous transmitting and reflecting RISs (STAR-RISs) are recently proposed to achieve 360° wireless coverage [9]. Compared to classical RISs, STAR-RISs can serve users located on both sides of their surface. STAR-RISs consist of elements that can produce both electric polarization and magnetization currents, which allows simultaneous control of the transmit and reflect incident signals towards the users located at different sides of the surface. Recently, a number of works have been reported incorporating NOMA and STAR-RIS in wireless networks [10]-[25]. The authors in [10] showed that the coverage can be significantly extended by integrating STAR-RISs into NOMA networks. The authors in [11] took advantage of STAR-RIS to simultaneously eliminate inter-cell interference and enhance the desired signals in NOMA enhanced coordinated multi-point transmission networks. In [12], 13 and 14, the authors maximized the weighted sum-rate for the STAR-RIS-assisted multiple-input multiple-output system, the sum secrecy rate for the STAR-RIS-assisted multiple-input single-output system, and the achievable sum-rate of STAR-RIS-NOMA system, respectively. The STAR-RIS in [15] is utilized for adjusting users' decoding order to efficiently mitigate the mutual interference between users and to extend the coverage of heterogeneous networks. In [16] and [17], the authors proposed different approximated mathematical channel models to investigate the outage probability (OP) performance for STAR-intelligent omini-surfaces based NOMA and STAR-RIS-NOMA multi-cell networks. In [18], the authors considered a realistic transmission and reflection coupled phase-shift model for STAR-RISs. The authors in [19]

M. Aldababsa is with the Department of Electrical and Electronics Engineering, Istanbul Gelisim University, 34310, Istanbul, Turkey. (e-mail: mhkaldababsa@gelisim.edu.tr).

A. Khaleel and E. Basar are with the Communications Research and Innovation Laboratory (CoreLab), Department of Electrical and Electronics Engineering, Koc University, Sariyer 34450, Istanbul, Turkey. (e-mail: akhaleel18@ku.edu.tr, ebasar@ku.edu.tr).

proposed a STAR-RIS partitioning algorithm for a STAR-RIS-NOMA network. It is designed to maximize the sum-rate and guarantee the quality-of-service requirements by assigning a proper number of STAR-RIS elements to each user. In [20] and [21], optimizations problems are considered to minimize the power consumption and maximum secrecy OP, respectively, for uplink STAR-RIS-NOMA networks. The authors in [22] investigated the resource allocation scheme in STAR-RIS-aided multi-carrier OMA and NOMA networks to maximize the sum-rate. In [23], a deep reinforcement learning-based algorithm is designed to maximize the energy efficiency for a STAR-RIS-NOMA network. The authors in [24] proposed practical phase-shift configuration strategies for STAR-RIS-NOMA networks with correlated phase shifts. In [25], the performance of STAR-RIS-NOMA networks is investigated in terms of OP and ergodic sum-rate.

To the best of the authors' knowledge, the studies of [3]-[4] assumed a simple scenario of two NOMA users, which might not be practical. Furthermore, the works of [7]-[8] assumed that each user receives the signals reflected from the RIS partition assigned to it only and without interference signals from the other partition, which is physically impossible. Moreover, the performance of STAR-RIS-NOMA networks in [10]-[25] is analyzed in terms of OP and sum-rate only, and no light has been shed on the BER performance aspect yet. These have motivated us to investigate the BER performance for STAR-RIS-NOMA networks, where BS communicates multiple non-orthogonal users with the assistance of a STAR-RIS. The main contributions of the paper can be summarized as follows. We analyze the BER performance of the STAR-RIS-NOMA network considering the subsurface mutual interference within the RIS transmission or reflection part in the cases of perfect and imperfect SIC. We derive the closed-form expressions of the BER for the users employing a BPSK modulation. Then, asymptotic analyses are carried out to provide further insight into BER behavior in the high signal-to-noise ratio (SNR) region. Finally, we verify our analytical results by Monte Carlo simulations, which demonstrate the superiority of the proposed network over the classical NOMA system.[1]

II. System Model

As illustrated in Fig. 1, we consider a STAR-RIS-NOMA network, in which a single-antenna BS communicates simultaneously K single-antenna users with the help of a STAR-RIS equipped with N passive elements. The K users $(\mathrm{U}_1, ..., \mathrm{U}_K)$ are deployed on both sides of the STAR-RIS, where K_t and K_r users are located in the transmission and reflection zones, respectively. The direct communication links between the BS and users are assumed to be unavailable due to natural or manmade obstacles and the STAR-RIS is deployed to provide alternative communication links for users

[1]*Notation:* Matrices and vectors are denoted by an upper and lower case boldface letters, respectively. $\mathbb{C}^{m\times n}$ denotes the set of matrices with dimension $m \times n$. $|\cdot|$, $\mathrm{E}[\cdot]$, and $(\cdot)^T$ represent the absolute value, expectation operator, and transpose operator, respectively. $f_X(x)$ denotes probability density function (PDF) of a random variable (RV) X. $\mathcal{CN}(\mu, \sigma^2)$ stands for the complex Gaussian distribution with mean μ and variance σ^2. $Q(\cdot)$ and $erf(\cdot)$ denote the Q-function and error function, respectively.

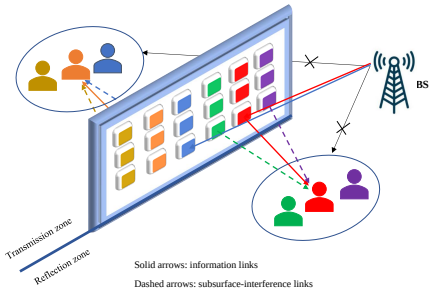


Fig. 1. A STAR-RIS-assisted NOMA system model.

through the transmission/reflection elements. The STAR-RIS adopts mode switching (MS) protocol, where each element can operate in full transmission or reflection mode. Thus, the STAR-RIS is partitioned into two main parts, where the first and second parts contain N_t transmitting and N_r reflecting elements to serve the users in transmission and reflection zones, respectively. Both parts of the RIS are partitioned into subsurfaces, where each subsurface is allocated to serve a specific user in the transmission or reflection zone. The BS-STAR-RIS link is assumed to follow Rayleigh fading channel model, where $\mathbf{h}_i \in \mathbb{C}^{N_i\times 1}$ denotes the BS-ith subsurface vector with N_i refers to the number of elements that belong to the ith subsurface in the transmission (t) or reflection (r) part of the STAR-RIS. $\mathbf{h}_i = \left[h_i^{(1)}, ..., h_i^{(n)}, ..., h_i^{(N_i)}\right]^T$ with $h_i^{(n)} = \sqrt{L_{BS}}\zeta_i^{(n)} e^{-j\phi_i^{(n)}}$ denoting the channel coefficient between the BS and nth STAR-RIS element in the ith subsurface, where L_{BS}, $\zeta_i^{(n)}$, and $\phi_i^{(n)}$ denote the path gain, channel amplitude, and channel phase, respectively, and $h_i^{(n)} \sim \mathcal{CN}(0, L_{BS})$. Likewise, the STAR-RIS-U_k link is assumed to follow Rayleigh fading channel model, where the channel vector between the ith subsurface in the transmission or reflection part of the STAR-RIS and U_k is denoted by $\mathbf{g}_{k,i} \in \mathbb{C}^{N_i\times 1}$, $\mathbf{g}_{k,i} = \left[g_{k,i}^{(1)}, ..., g_{k,i}^{(n)}, ..., g_{k,i}^{(N_i)}\right]^T$, $g_{k,i}^{(n)} = \sqrt{L_{SU,k}}\eta_{k,i}^{(n)} e^{-j\Phi_{k,i}^{(n)}}$ denotes the channel coefficient between nth RIS element in the ith subsurface and U_k, where $L_{SU,k}$, $\eta_{k,i}^{(n)}$, and $\Phi_{k,i}^{(n)}$ denote the path gain, channel amplitude, and channel phase, respectively, and $g_{k,i}^{(n)} \sim \mathcal{CN}(0, L_{SU,k})$. The transmission and reflection coefficients for the ith subsurface in the transmission and reflection parts of the STAR-RIS are denoted by the entries of the diagonal matrix $\mathbf{\Theta}_i \in \mathbb{C}^{N_i\times N_i}$, for the nth element we have $\Theta_i^{(n,n)} = e^{j\theta_i^{(n)}}$, where $\theta_i^{(n)} \in [0, 2\pi)$. In the considered setup, the users are ordered according to their channel gains such U_1 and U_K are the weakest and strongest channel gains, respectively. Thus, the power allocation are inversely ordered as $a_1 \geq ... \geq a_K$. Given, P is the BS transmit power, x_k and a_k are U_k's symbol and power allocation factor, respectively, $\mathrm{E}\left[|x_k|^2\right] = 1$, $\sum_k a_k = 1$. Then, the BS transmits the superimposed signal $x = \sum_k \sqrt{a_k P} x_k$ to all users and the received signal at U_k is

$$y_k = \mathbf{g}_k^T \mathbf{\Theta}_k \mathbf{h}_k x + \sum_i \mathbf{g}_{k,i}^T \mathbf{\Theta}_i \mathbf{h}_i x + n_k, \tag{1}$$

where $\sum_i \mathbf{g}_{k,i}^T \mathbf{\Theta}_i \mathbf{h}_i x$ refers to subsurfaces mutual interference within the transmission or reflection part of the RIS and n_k denotes the complex additive white Gaussian noise

(AWGN) sample with zero mean and variance σ^2 at U_k, i.e., $n_k \sim \mathcal{CN}(0, \sigma^2)$. Notably, U_1 has the highest allocated power coefficient, and thus it does not perform the SIC process. It detects its signal directly by considering other users' symbols as noise and implement maximum likelihood detection (MLD). On the other hand, U_k needs the SIC process to detect and subtract $\{1, ..., k-1\}$'s signals and then it implements MLD to detect its signal. Accordingly, the detected $\hat{x}_k$ can be stated as

$$\hat{x}_k = \arg\min_i \left\{ \left| y_k^* - \sqrt{a_k P} \mathbf{g}_k^T \mathbf{\Theta}_k \mathbf{h}_k x_k^{(i)} \right|^2 \right\}, \quad (2)$$

where $y_k^* = y_k - \sum_{j=1}^{k-1} \sqrt{a_j P} \mathbf{g}_k^T \mathbf{\Theta}_k \mathbf{h}_k \hat{x}_j$ and $x_k^{(i)}$ denotes ith element in the set of x_k constellation.

III. Bit Error Rate Analysis

The average bit error probability for U_k is given by

$$\mathcal{P}_{e,k} = \int_0^\infty \mathcal{P}(e|\varphi_k) f_{\varphi_k}(x) dx, \quad (3)$$

where $\varphi_k = |\mathbf{g}_k^T \mathbf{\Theta}_k \mathbf{h}_k|$, $\mathcal{P}(e|\varphi_k)$ and $f_{\varphi_k}(x)$ denote absolute cascaded channel, conditional BER for U_k in AWGN channel and the PDF of the cascaded channel φ_k, respectively. In what follows, we derive $\mathcal{P}(e|\varphi_k)$ and $f_{\varphi_k}(x)$ in Lemmas 1 and 2, respectively, then we obtain $\mathcal{P}_{e,k}$ in the cases of absence and presence of SIC error in Propositions 1 and 2, respectively.

Lemma 1. *The BER for U_k in AWGN can be given by*

$$\mathcal{P}\left(e|\varphi_k\right) = \sum_i \mathcal{P}\left(A_k^{(i)}\right) Q\left(A_k^{(i)} \varphi_k \sqrt{\varrho_k \gamma}\right), \quad (4)$$

where $A_k^{(i)}$ denotes ith combination in $A_k \in \left\{\sqrt{a_k P} \pm ... \pm \sqrt{a_K P}\right\}$ and $\mathcal{P}\left(A_k^{(i)}\right) = 2^{k-K}$. Additionally, $\gamma \triangleq \frac{P}{\sigma^2}$ is the signal-to-noise ratio (SNR), $\varrho_k = \left(1 + L_k \left(N_\chi - N_k\right) \gamma / P\right)^{-1}$. Here, $\chi \in \{t, r\}$, $L_k = L_{BS} L_{SU,k} = d_{BS}^{-\alpha_{BS}} d_{SU,k}^{-\alpha_{SU}}$ is the overall path gain of the BS-RIS-U_k link, where (α_{BS}, d_{BS}), and $(\alpha_{SU}, d_{SU,k})$ refer to (path loss exponents, distances) associated with the BS-RIS and RIS-U_k links, respectively.

Proof. According to the central limit theorem (CLT), for large number of RIS elements, $\sum_i \mathbf{g}_{k,i}^T \mathbf{\Theta}_i \mathbf{h}_i x$ in (1) converges to Gaussian RV, i.e., $\sum_i \mathbf{g}_{k,i}^T \mathbf{\Theta}_i \mathbf{h}_i x \sim \mathcal{CN}\left(0, L_k \left(N_\chi - N_k\right)\right)$. Then, $y_k = \mathbf{g}_k^T \mathbf{\Theta}_k \mathbf{h}_k x + w_k$, where $w_k \sim \mathcal{CN}(0, \sigma^2 + L_k \left(N_\chi - N_k\right))$. Following same derivation steps in [3]-[4], the BER for U_k in AWGN can be achieved in (4). ∎

Lemma 2. *The PDF of φ_k is given by*

$$f_{\varphi_k}(x) = \frac{1}{\sqrt{2\pi v_k}} \exp\left(-\frac{\left(x - \mu_k\right)^2}{2 v_k}\right), \quad (5)$$

where $\mu_k = \frac{\pi}{4} \sqrt{L_k} N_k$ and $v_k = \left(1 - \frac{\pi^2}{16}\right) L_k N_k$.

Proof. The SNR can be maximized by letting $\theta_k^{(n)} = \phi_k^{(n)} + \Phi_k^{(n)}$. Thus, φ_k corresponds to the sum of product of two independent Rayleigh RVs. According to the CLT, when $N_k \to \infty$, φ_k follows Gaussian distribution, $\varphi_k \sim \mathcal{N}\left(\mu_k, v_k\right)$. Hence, the PDF of φ_k can be finally expressed as in (5). ∎

Proposition 1. *In the perfect SIC case, the BER of U_k is*

$$\mathcal{P}_{e,k} \approx \frac{\exp\left(-\frac{2cv_k + \mu_k^2}{2v_k}\right)}{\sqrt{2v_k}} \sum_i \mathcal{P}\left(A_k^{(i)}\right) \exp\left(\frac{\left(bA_k^{(i)}\sqrt{\varrho_k\gamma}v_k - \mu_k\right)^2}{4a\left(A_k^{(i)}\right)^2 \varrho_k \gamma v_k^2 + 2v_k}\right) \sqrt{\frac{v_k}{4\left(A_k^{(i)}\right)^2 \varrho_k \gamma v_k + 2}} \left(1 + erf\left(\sqrt{\frac{\left(bA_k^{(i)}\sqrt{\varrho_k\gamma}v_k - \mu_k\right)^2}{4a\left(A_k^{(i)}\right)^2 \varrho_k \gamma v_k^2 + 2v_k}}\right)\right), \quad (6)$$

where $(a, b, c) = (0.3842, 0.7640, 0.6964)$ are the fitting coefficients used by Lopez-Benitez and Casadevall in approximating Q-function [26].

Proof. A tighter and more tractable approximation of Q-function in Lemma 1 can be given by Lopez-Benitez and Casadevall. The integral obtained by substituting this approximation and Lemma 2 into (3) can be written in terms of error function [27, Eq. (3.322.2)]. Therefore, the BER of U_k can be finally stated in (6). ∎

In general scenarios, detection errors can appear at any step of the SIC process. Proposition 2 considers a special case (two-user scenario, where U_1 and U_2 are located at the transmission and reflection zones, respectively), which can be generalized for K users.

Proposition 2. *In the presence of SIC error, the BER for U_1 and U_2 can be given by*

$$\mathcal{P}_{e,1}^{sic} = \mathcal{P}_{e,1} \text{ and } \mathcal{P}_{e,2}^{sic} \approx \mathcal{P}_{e,2} \mathcal{P}\left(x_1^c\right) + 0.5\left(1 - \mathcal{P}\left(x_1^c\right)\right), \quad (7)$$

where $\mathcal{P}\left(x_1^c\right)$ refers to average bit error probability for U_1 when its signal is detected at U_2 and can be calculated from (6) *with related parameters of φ_2.*

Proof. U_1 does not carry out SIC process and hence the BER for U_1 is calculated form (6), i.e., $\mathcal{P}_{e,1}^{sic} = \mathcal{P}_{e,1}$. On the other hand, U_2 performs SIC process, and hence the BER for U_2 should be considered for both correct and erroneous SIC cases, $\mathcal{P}_{e,2}^{sic} = \mathcal{P}\left(x_2/x_1^c\right)\mathcal{P}\left(x_1^c\right) + \mathcal{P}\left(x_2/x_1^e\right)\mathcal{P}\left(x_1^e\right)$. Here, $\mathcal{P}\left(x_1^c\right)$ and $\mathcal{P}\left(x_1^e\right)$ denote average bit error probability for correct and erroneous detection of x_1 at U_2, respectively. $\mathcal{P}\left(x_2/x_1^c\right)$ and $\mathcal{P}\left(x_2/x_1^e\right)$ denote average bit error probability for x_2 when x_2 is correctly and erroneously detected at U_2, respectively. $\mathcal{P}\left(x_1^c\right)$ is calculated from (6) with related parameters of φ_2, and hence $\mathcal{P}\left(x_1^e\right) = 1 - \mathcal{P}\left(x_1^c\right)$. Form (6), $\mathcal{P}\left(x_2/x_1^c\right)$ can be also found, i.e., $\mathcal{P}\left(x_2/x_1^c\right) = \mathcal{P}_{e,2}$ and $\mathcal{P}\left(x_2/x_1^e\right)$ is very close to the worst case, i.e., $\mathcal{P}\left(x_2/x_1^e\right) \approx 0.5$. ∎

It is difficult to get an insight from the BER expressions in Propositions. In corollary 1, we examine the BER behavior in the high SNR regime.

Corollary 1. *In high SNR region, the BER can be given as*

$$\mathcal{P}_{e,k}^{\infty} \approx \frac{\exp\left(-\frac{2cv_k+\mu_k^2}{2v_k}\right)}{\sqrt{2v_k}} \sum_i \mathcal{P}\left(A_k^{(i)}\right) \times \exp\left(\frac{\left(bA_k^{(i)}\sqrt{\varpi}v_k-\mu_k\right)^2}{4a\left(A_k^{(i)}\right)^2\varpi v_k^2+2v_k}\right)\sqrt{\frac{v_k}{4\left(A_k^{(i)}\right)^2\varpi v_k+2}} \times\left(1+erf\left(\sqrt{\frac{\left(bA_k^{(i)}\sqrt{\varpi}v_k-\mu_k\right)^2}{4a\left(A_k^{(i)}\right)^2\varpi v_k^2+2v_k}}\right)\right), \quad (8)$$

where $\varpi = \left(L_k\left(N_\chi - N_k\right)/P\right)^{-1}$.

Proof. Let $\varpi = \varrho_k\gamma$, when $\gamma \to \infty$, $\varpi = \left(L_k\left(N_\chi - N_k\right)/P\right)^{-1}$, substituting in (6) we obtain (8). ■

From Corollary 1, it can be noticed that, due to the subsurface interference, the asymptotic BER does not depend on the SNR. The BER reaches a fixed value (error floor) in the high SNR region, which indicates that the diversity gain is zero.

IV. Numerical Results

In this section, Monte Carlo simulations are presented to show the performance of the STAR-RIS-NOMA system, and to validate the BER analytical results. Unless stated otherwise, we assume $P = 1$ and $\alpha_{BS} = \alpha_{SU} = 2$. We compare the proposed system with the classical NOMA system by considering the same simulation parameters, and the BS-U_k path gain is modelled as $L_k = d_k^{-\alpha}$, where d_k is the BS-U_k distance and $\alpha = 2$ is the path loss exponent. Fig. 2(a)-(b) show the BER performance versus SNR in the case of perfect SIC for two-user scenario, where each user is located at different side of RIS. It can be clearly seen that the obtained analytical results perfectly match the simulations curves. It can be also seen that both users achieve better BER performance as the number of RIS elements increases. Compared to classical NOMA system, Fig. 2(b) shows that STAR-RIS NOMA (U_2) achieves 20 dB, 25 dB, and 29 dB performance gains for $N_1 = 25, 50$ and 75, respectively at BER of 10^{-3}. Fig. 3 shows the BER performance versus SNR for U_2 in the cases of perfect and imperfect SIC. It is observed that the BER performance gets worse in the presence of SIC error even when the number of RIS elements increases. However, when a_2 decreases (a_1 increases), the SIC error decreases. This is because increasing a_1 increases the probability of detecting its signal correctly and results in a reduction of SIC error. Fig. 4 depicts the BER performance versus number of RIS elements for different power allocation coefficients. It is observed that U_1 is more sensitive to the change in the power allocation over the change of the number of RIS elements. This is because U_1 does not carry out any SIC process, and hence changes in the power allocation result in variations in the interference level caused by U_2. For instance, an increment of 0.1 in the power allocation makes U_1 need 13 fewer elements to achieve the same BER of 10^{-3}. On the other side, U_2 needs 3 elements more to achieve the same BER of 10^{-3}. Fig. 5 plots the BER

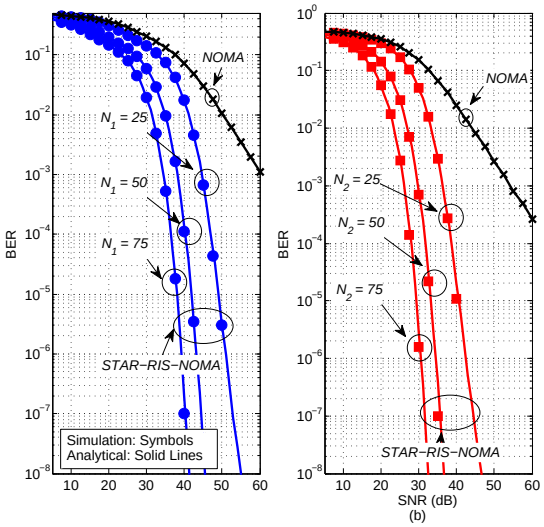


Fig. 2. The BER versus SNR for (a) U_1 and (b) U_2 in the perfect SIC case, $(a_1, a_2) = (0.7, 0.3)$ and $\left(d_{BS}, d_{SU,1}, d_{SU,2}\right) = (50, 6, 4)$ m

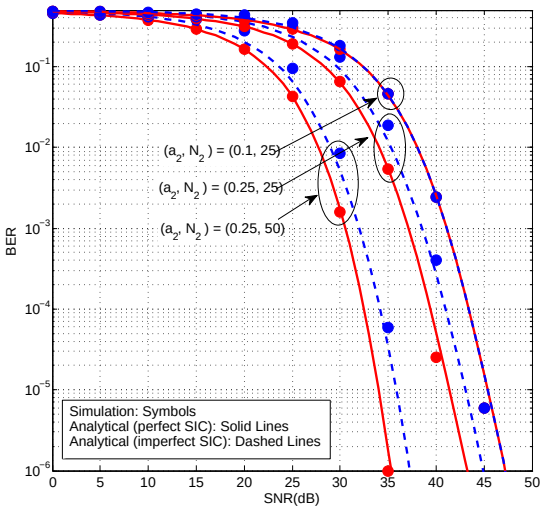


Fig. 3. The BER performance versus SNR for U_2 in the perfect and imperfect SIC cases.

performance versus SNR for three-user scenario, where U_1 and U_2 are located at the transmission zone and U_3 is located at the reflection zone. Notice that BER performance enhances as the number of RIS elements increases. However, when SNR increases, the BERs for U_1 and U_2 reach an error floor due to the mutual subsurface-interference. On the other hand, the BER for U_3 does not reach error floor since U_3 does not suffer from any mutual subsurface-interference.

V. Conclusion

We have examined the BER performance of STAR-RIS-NOMA network, in which a STAR-RIS utilizes the MS protocol to provide communication between a BS and multiple NOMA users located on both its sides. We have derived closed-form expressions for BER in both perfect and imperfect SIC cases. Then, asymptotic analyses have been carried out to provide further insights into the error rate behavior in the high SNR region. Based on the numerical results, we conclude that

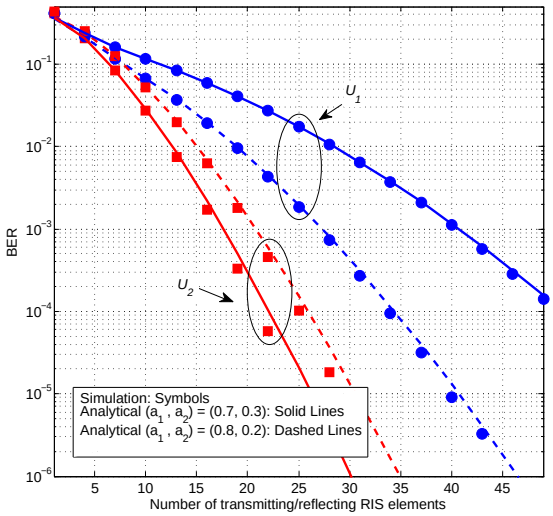


Fig. 4. The BER performance versus number of transmitting/reflecting elements for different power allocation coefficients and $\gamma = 40$ dB.

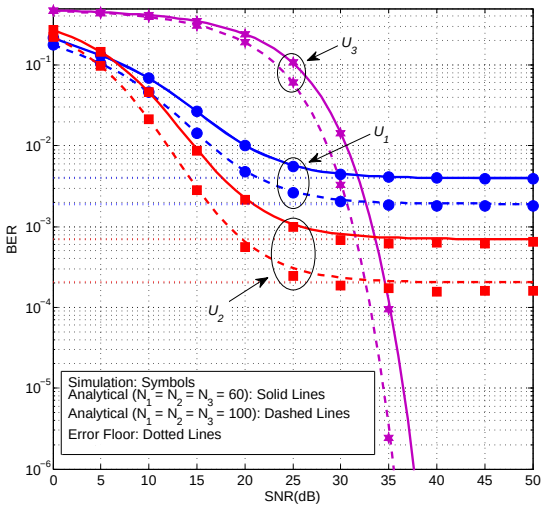


Fig. 5. The BER versus SNR for three-user scenario, $(a_1, a_2, a_3) = (0.75, 0.248, 0.002)$ and $\left(d_{BS}, d_{SU,1}, d_{SU,2}, d_{SU,2}\right) = (20, 3, 2.5, 2)$ m.

the BER performance enhances with increasing numbers of RIS elements. Moreover, in the case of imperfect SIC, the BER performance gets worse. On the other hand, in the case of perfect SIC, the users achieve diversity gain. Furthermore, the farthest user is more sensitive to changes in the power allocation over the change of numbers of RIS elements. Finally, it has been shown that the BER performance of STAR-RIS-NOMA outperforms that of the classical NOMA system and STAR-RIS based NOMA can be useful candidate for future systems. For a future work, the BER analysis provided here can be extended to the scenario where the STAR-RIS is partitioned between multiple users, and the aim is to find the minimum number of elements needs to be allocated for each user to guarantee a minimum BER threshold for all users.

REFERENCES

[1] W. U. Khan *et al.*, "Spectral efficiency optimization for next generation NOMA-enabled IoT networks," *IEEE Trans. Veh. Techno.*, vol. 69, no. 12, pp. 15284-15297, Dec. 2020.

[2] S. M. R. Islam *et al.*, "Power-domain non-orthogonal multiple access (NOMA) in 5G systems: potentials and challenges," *IEEE Commun. Surveys & Tuts.*, vol. 19, no. 2, pp. 721-742, 2nd quarter 2017.

[3] F. Kara and H. Kaya, "BER performances of downlink and uplink NOMA in the presence of SIC errors over fading channels", *IET Commun.*, vol. 12, no. 15, pp. 1834-1844, Aug. 2018.

[4] T. Assaf *et al.*, "Exact Bit Error-Rate Analysis of Two-User NOMA Using QAM with Arbitrary Modulation Orders", *IEEE Commun. Lett.*, vol. 24, no. 12, pp. 1–1, Aug. 2020.

[5] D. Wan *et al.* "A Simple multicarrier transmission technique combining transmit diversity and data multiplexing for non-orthogonal multiple access" *IEEE Trans. Veh. Technol.*, vol. 70, no. 7, pp. 7216-7220, Jul. 2021.

[6] Z. Zhu *et al.* "Resource allocation for intelligent reflecting surface assisted wireless powered IoT systems with power splitting," *IEEE Trans. Cmmun.*, vol. 21, no. 5, pp. 2987-2998, May 2022.

[7] V. C. Thirumavalavan and T. S. Jayaraman, "BER Analysis of Reconfigurable Intelligent Surface Assisted Downlink Power Domain NOMA System", *Int. Conf. Commun. Syst. Netw.*, pp. 519-522, Jan. 2020.

[8] L. Bariah *et al.*, "Large Intelligent Surface-Assisted Nonorthogonal Multiple Access for 6G Networks: Performance Analysis," *IEEE Internet of Things Journal*, vol. 8, no. 7, pp. 5129-5140, April 2021.

[9] Y. Liu *et al.*, "STAR: Simultaneous transmission and reflection for 360 coverage by intelligent surfaces," *IEEE Wire. Commun.*, vol. 28, no. 6, pp. 102-109, December 2021.

[10] C. Wu *et al.*, "Coverage characterization of STAR-RIS networks: NOMA and OMA," *IEEE Commun. Lett.*, vol. 25, no. 9, pp. 3036-3040, Sept. 2021.

[11] T. Hou *et al.*, "A jointly design for STAR-RIS enhanced NOMA-CoMP networks:a simultaneously-signal-enhancement-and-cancellation-based (SSECB) design," May 2021. [Online]. Available: https://arxiv.org/abs/2105.00404v2..

[12] H. Niu *et al.*, "Weighted sum rate optimization for STAR-RIS-assisted MIMO system," *IEEE Trans. Veh. Technol.*, vol. 71, no. 2, pp. 2122-2127, Feb. 2022.

[13] H. Niu *et al.*, "Simultaneous transmission and reflection reconfigurable intelligent surface assisted secrecy MISO networks," *IEEE Commun. Lett.*, vol. 25, no. 11, pp. 3498-3502, Nov. 2021.

[14] J. Zuo *et al.*, "Joint design for simultaneously transmitting and reflecting (STAR) RIS assisted NOMA systems," June 2021. [Online]. Available: https://arxiv.org/abs/2106.03001v1..

[15] W. Ni *et al.*, "STAR-RIS enabled heterogeneous networks: ubiquitous NOMA communication and pervasive federated learning," June 2021. [Online]. Available: https://arxiv.org/abs/2106.08592v2..

[16] C. Zhang *et al.*, "STAR-IOS Aided NOMA Networks: Channel Model Approximation and Performance Analysis," *IEEE Trans. Wire. Commun.*, Feb. 2022.

[17] Z. Xie *et al.*, "STAR-RIS aided NOMA in multi-cell networks: a general analytical framework with Gamma distributed channel modeling," Aug. 2021. [Online]. Available: https://arxiv.org/abs/2108.06704v1..

[18] Y. Liu *et al.*, "Simultaneously Transmitting and Reflecting (STAR)-RISs: A coupled Phase-Shift Model," Oct. 2021. [Online]. Available: https://arxiv.org/abs/2110.02374v1..

[19] M. Aldababsa, A. Khaleel and E. Basar, "Simultaneous transmitting and reflecting intelligent surfaces-empowered NOMA network," Oct. 2021. [Online]. Available: https://arxiv.org/abs/2110.05311v1..

[20] J. Zuo *et al.*, "Uplink NOMA for STAR-RIS networks," Nov. 2021. [Online]. Available: https://arxiv.org/abs/2110.05686v2..

[21] Z. Zhang *et al.*, "On the secrecy design of STAR-RIS assisted uplink NOMA networks," Nov. 2021. [Online]. Available: https://arxiv.org/abs/2111.02642v1..

[22] C. Wu *et al.*, "Resource allocation in STAR-RIS-aided networks: OMA and NOMA," *IEEE Trans. Wire. Commun.*, March 2022.

[23] Y. Guo *et al.*, "Energy-efficient design for a NOMA assisted STAR-RIS network with deep reinforcement learning," Nov. 2021. [Online]. Available: https://arxiv.org/abs/2111.15464v1..

[24] J. Xu *et al.*, "STAR-RISs: A correlated T&R phase-shift model and practical phase-shift configuration strategies," Dec. 2021. [Online]. Available: https://arxiv.org/abs/2112.00299v1..

[25] X. Yue *et al.*, "Simultaneously transmitting and reflecting reconfigurable intelligent surface assisted NOMA networks," Dec. 2021. [Online]. Available: https://arxiv.org/abs/2112.01336v1..

[26] M. López-Benítez and F. Casadevall, "Versatile, accurate, and analytically tractable approximation for the Gaussian Q-Function," *IEEE Trans. Commun.*, vol. 59, no. 4, pp. 917-922, April 2011.

[27] IS. Gradshteyn and IM. Ryzhik, *Table of integrals, series, and products*, 7th Ed. Academic Press: San Diego, CA, 2007.